Finite-Orbit-Width Effect and the Radial Electric Field in Neoclassical Transport Phenomena

S. Satake 1), M. Okamoto 1), N. Nakajima 1), H. Sugama 1), M. Yokoyama 1), and C. D. Beidler 2)

1) National Institute for Fusion Science, Toki, Japan
2) Max-Planck-Institut für Plasmaphysik, Greifswald, Germany

e-mail contact of main author : satake.shinsuke@nifs.ac.jp

Abstract. Modeling and detailed simulation of neoclassical transport phenomena both in 2D and 3D toroidal configurations are shown. The emphasis is put on the effect of finiteness of the drift-orbit width, which brings a non-local nature to neoclassical transport phenomena. Evolution of the self-consistent radial electric field in the framework of neoclassical transport is also investigated. The combination of Monte-Carlo calculation for ion transport and numerical solver of ripple-averaged kinetic equation for electrons makes it possible to calculate neoclassical fluxes and the time evolution of the radial electric field in the whole plasma region, including the finite-orbit-width(FOW) effects and global evolution of geodesic acoustic mode (GAM). The simulation results show that the heat conductivity around the magnetic axis is smaller than that obtained from standard neoclassical theory and that the evolution of GAM oscillation on each flux surface is coupled with other surfaces if the FOW effect is significant. A global simulation of radial electric field evolution in a non-axisymmetric plasma is also shown.

1. Introduction

Neoclassical(NC) transport theory has been successfully established under the assumption of the local transport model(small-orbit-width (SOW) limit)[1,2]. However, there are some cases in recent experiments where the assumption is not valid, for example, at the internal transport barrier(ITB) and in the core region of tokamak where potato orbits[3] appear. The potato width becomes several tens % of the plasma minor radius in a reversed-shear configuration, and to evaluate transport level in such cases the finite-orbit-width(FOW) effect of trapped particles should be considered. Neoclassical transport theory for 3-dimensional stellarator configurations has also been considered in the SOW-limit[4,5]. The drift orbits in stellarators are much complicated compared to those in tokamaks. Though the orbit widths of ripple-trapped particles are small, transit particles in stellarators have large orbit scales, and energetic particles trapped helically are easy to lose from the confinement region. In order to take account of those particles in NC transport calculation, conventional analytical method is hard to apply, and global properties of particle motion should be taken into account.

Another interest in recent study on NC transport is the formation of the radial electric field E_r. Since the lowest-order NC flux is intrinsic ambipolar in tokamaks, the higher-order terms appeared from the FOW effect must be retained to evaluate the time evolution of E_r. In stellarators, the radial flux is non-ambipolar even in the lowest order. Because NC fluxes in non-axisymmetric plasmas are sensitive to electric field, determination of the self-consistent ambipolar electric field is one of the main task of neoclassical theory.

However, the role of the FOW effects in the evolution of radial electric field has not been investigated in detail.

To carry out a general and detailed research on neoclassical transport phenomena including the finite-orbit-width effects and radial electric field, we develop a numerical transport simulation code FORTEC-3D using the δf Monte-Carlo method[6,7]. It solves the time evolution of neoclassical fluxes as well as the self-consistent radial electric field, in multidimensional MHD equilibrium configurations obtained from VMEC[8]. The original FORTEC has been developed to solve NC transport for ions in tokamaks, in which the electron particle flux Γ_e is negligible to determine ambipolar E_r. In non-axisymmetric cases Γ_e is comparable to Γ_i and is needed to calculate the evolution of ambipolar electric field. To reduce the time consumption for simulation, we adopt a hybrid model. While the ion transport is solved by the δf method, the electron flux is obtained from GSRAKE[9], a numerical solver of ripple-averaged kinetic equation. Thus FORTEC-3D enables us to investigate neoclassical transport and the evolution of radial electric field including the FOW effects of ions in general 3D configurations, from a microscopic point of view.

The remainder of the paper is organized as follows. In Sec. 2, formulation of δf Monte-Carlo method and our simulation modeling are explained. In Sec. 3, NC transport simulation in a tokamak configuration is shown. It is shown that the geodesic-acoustic-mode (GAM) oscillation in tokamak is affected by the FOW effects. The evolution of E_r on each flux surface is found to be coupled if the banana width is large. Effects of potato particles on transport are also shown. We have developed an extended transport theory including the FOW effects[10]. From the new neoclassical theory we show that the potato orbits around the axis plays an important role to the decreasing tendency of ion heat conductivity around the magnetic axis. In Sec. 3, a test calculation of NC transport in a LHD-like configuration in combination with GSRAKE is presented. The relaxation process of GAM oscillation toward ambipolar steady state is simulated precisely.

2. Simulation model

Consider a general toroidal plasma in the magnetic coordinates (ρ, θ, ζ), where $\rho = \sqrt{\psi/\psi_a}$ is a normalized radial coordinate and ψ_a is the toroidal flux label on the boundary. To solve the time development of a plasma distribution function in the phase space $(\rho, \theta, \zeta, \mathcal{K} = v^2, \mu = mv_\perp^2/2B)$, the linearized drift kinetic equation

$$\frac{D\delta f}{Dt} \equiv \left[\frac{\partial}{\partial t} + \dot{\mathcal{K}}\frac{\partial}{\partial \mathcal{K}} + (\mathbf{v}_\parallel + \mathbf{v}_d)\cdot\nabla - C_{tp}(\ , f_M)\right]\delta f = -\mathbf{v}_d\cdot\left(\nabla f_M - \frac{e\mathbf{E}_\rho}{T}\right) f_M + \mathcal{P} f_M \quad (1)$$

is considered. Here, $\mathbf{E}_\rho = -d\Phi/d\rho\nabla\rho$ is radial electric field, $\mathbf{v}_d$ is the drift velocity of a guiding center, and $f_M = f_M(\rho, \mathcal{K})$ is Maxwellian of a flux-surface function. The linearized test-particle collision operator C_{tp} is implemented numerically as a random kick in the velocity space. The field-particle collision operator $\mathcal{P} f_M$ is defined so as to satisfy the conservation lows for collision operator

$$\int (C_{tp} + \mathcal{P} f_M)\mathcal{M}_{\{0,1,2\}} d\mathbf{v} \quad = \quad 0, \quad (2)$$

where $\mathcal{M}_0 = 1$, $\mathcal{M}_1 = \mathbf{v}$, and $\mathcal{M}_2 = \mathcal{K}$, respectively[11]. The use of the operator which acts correctly as the linearized Fokker-Planck collision term is an advantage of our code to apply it to general toroidal geometry. Because of the break of the momentum-conservation low, it is known that the pitch-angle scattering operator, though it is a good approximation for neoclassical theory in helical systems, cannot be simply applied to the transport analysis in axisymmetric plasmas[12]. Note also that in the δf formulation, the FOW effect is included in the term $\mathbf{v}_d \cdot \nabla \delta f$, which is usually dropped in standard local transport models. We adopted the 2-weight scheme[6] to solve eq. (1) by Monte-Carlo method. Two weights w and p which satisfy the relation $wg = \delta f$, $pg = f_M$ are introduced, where g is the distribution function of simulation markers. Each marker follows the track in the phase space according to the lhs of eq. (1), that is, $Dg/Dt = 0$ is satisfied. Then the problem is reduced to solve the evolution of weights for each markers

$$\dot{w} = \frac{p}{f_M}\left[-\mathbf{v}_d \cdot \left(\nabla - \frac{e\mathbf{E}_\rho}{T}\right) + \mathcal{P}\right] f_M, \tag{3}$$

$$\dot{p} = \frac{p}{f_M}\mathbf{v}_d \cdot \left(\nabla - \frac{e\mathbf{E}_\rho}{T}\right) f_M. \tag{4}$$

We have also adopted a weight averaging technique to suppress the dispersion spreading of the weight fields[13].

The self-consistent evolution of the radial electric field is solved according to

$$\left(\langle|\nabla\rho|^2\rangle + \left\langle \frac{c^2}{v_A^2}|\nabla\rho|^2 \right\rangle\right) \epsilon_0 \frac{\partial E_\rho(\rho,t)}{\partial t} = -e\left(Z_i\Gamma_i^{neo} - \Gamma_e^{neo}\right), \tag{5}$$

where the ion particle flux is obtained from $\Gamma_i^{neo} = \langle \int d^3\mathbf{v}\ \dot{\rho}\ \delta f_i \rangle$. In tokamak cases, Γ_e^{neo} is negligible since $|\Gamma_e/\Gamma_i| \sim O(\sqrt{m_e/m_i})$. In non-axisymmetric cases, however, Γ_e^{neo} is comparable to Γ_i^{neo} and the balance between these two fluxes determines the ambipolar E_r. Since ion and electron fluxes are strongly dependent on E_r in the collisionless $1/\nu$ regime and the ambipolar condition $\Gamma_i(E_r) = \Gamma_e(E_r)$ sometimes has a multiple solution, we need a proper evaluation for Γ_e as well as Γ_i in order to investigate important phenomena in NC transport in stellarators such as time evolution and bifurcation of electric field. However, solving both ion and electron transport by δf scheme is not practical way because the orbit time scales of two species are too separated, and because it is expected that the FOW effect on transport is significant only for ions. In FORTEC-3D only the ion part is solved by using the δf method. The table of $\Gamma_e(E_\rho, \rho)$ for a given profile is prepared by GSRAKE, and Γ_e is referred from the table at each time step in solving eq. (5) in FORTEC-3D. GSRAKE is designed to give a general solution for ripple-averaged kinetic equation. The solution is valid throughout the entire long-mean-free-path (LMFP) regime. It is applicable to general, multi-helicity 3-dimensional configurations in which the magnetic field strength is given in a form

$$B = B_0 + \sum_{n=0}^{\infty} B_{0,n}(\rho)\cos n\zeta + \sum_{m=1}^{\infty}\sum_{n=-\infty}^{\infty} B_{m,n}(\rho)\cos(n\zeta - m\theta). \tag{6}$$

In our simulation system, the table of Fourier components of B are extracted from MHD equilibrium field solved by VMEC, and it is transfered to FORTEC-3D and GSRAKE. The

adaptability of GSRAKE to transport calculation in LHD plasmas has been benchmarked by comparing other numerical codes or analytical expressions previously[9].

Adopting the hybrid model, our simulation system is capable of solving neoclassical transport in general 2D and 3D configurations without missing the important role of the FOW effects of ions, within a practical calculation time. A typical simulation using 50 million markers in 3D configuration takes 20 hours to run a simulation to reach a steady state solution. It also enables us to investigate neoclassical transport dynamics in the whole plasma region from a microscopic point of view. The issues to be interested in with FORTEC-3D code are (1) the FOW effects on neoclassical transport (2) the propagation and damping of GAM oscillation in the entire plasma region (3) the effects of direct orbit-loss or some external sources and (4) precise simulation of the bifurcation phenomena and evolution of ambipolar E_r field in non-axisymmetric systems. In the following chapter our recent simulation results in tokamak and a LHD-like configuration are shown.

3. Transport simulation in 2D configurations

It has been revealed that the NC ion heat conductivity χ_i calculated by Monte-Carlo method decreases in the near-axis region of tokamaks[6,14,15]. To explain this, we have developed a new transport formulation for axisymmetric plasma to include the large-scale orbital properties of potato particles into NC theory[10]. It is based on Lagrangian description of drift-kinetic equation[16], in which the kinetic equation is solved in the phase space of the constants of motion $(\mathcal{E}, \mu, \langle\psi\rangle)$ in the collisionless limit. Here, $\mathcal{E}$ is the total energy, μ is the magnetic moment, and $\langle\psi\rangle$ is averaged radial position of guiding-center motion. The reduced drift-kinetic equation for the averaged distribution function $\bar{f}(\mathbf{z}) = \bar{f}(\mathcal{E}, \mu, \langle\psi\rangle)$ is as follows

$$\frac{\partial \bar{f}}{\partial t} = \frac{1}{J_c}\frac{\partial}{\partial \mathbf{z}} \cdot J_c \frac{\nu(\mathcal{E}, \langle\psi\rangle)}{2} \left[\left\langle \frac{\partial \mathbf{z}}{\partial \mathbf{v}} \cdot \mathsf{V} \cdot \frac{\partial \mathbf{z}}{\partial \mathbf{v}} \right\rangle \frac{\partial \bar{f}}{\partial \mathbf{z}} - \left\langle \frac{m u_\parallel}{T} \frac{\partial \mathbf{z}}{\partial \mathbf{v}} \cdot \mathbf{w} f_M \right\rangle \right] \tag{7}$$

where $\mathsf{V}(\mathbf{v}) = v^2 \mathsf{I} - \mathbf{v}\mathbf{v}$, $\mathbf{w} = v^2 \mathbf{b} - v_\parallel \mathbf{v}$, ν is collision frequency, and J_c is Jacobian. The rhs of eq.(7) describes the orbit-averaged collision operator, and $\langle \cdots \rangle$ is the orbit averaging operator. This equation can be interpreted as a description of the diffusion process of averaged radial position of particles by collisions. Since the orbit average is taken along real orbit, orbital properties of fat potato particles are included in the formulation. Equation (7) is solved by expanding $\bar{f} = \bar{f}_0 + \bar{f}_1 + \cdots$ and calculate the non-vanishing lowest order $\partial \bar{f}/\partial t$ in the second order. The final solution is obtained in the form of transport coefficients in an usual manner such as D_i and χ_i. The details of how to solve eq. (7) numerically is summarized in [10].

Typical potato orbit width is estimated as $\Delta_p \sim (q^2 \rho_i^2 R_0)^{1/3}$, where ρ_i is ion Larmor radius. Therefore, Δ_p becomes larger in reversed-shear configuration where $q \gg 1$ around the magnetic axis. To see the dependence of χ_i on Δ_p we show in Fig. 1 the example of calculation of χ_i in two configurations, one is a normal-shear case $q_{axis} = 1.5$, $q_{edge} = 4$ and $\Delta_p \simeq 0.08$, and the other is a reversed-shear case $q_{axis} = 8$, $q_{min} = 1.5$ at $r = 0.5$, $q_{edge} = 4$, and $\Delta_p \simeq 0.18$ respectively. The results are compared with the fitting formula of neoclassical theory in the standard local analysis[17], and the result from FORTEC-3D for the reversed-shear case. As shown in other Monte-Carlo simulations, χ_i obtained from

Lagrangian theory decreases in the near-axis region and the decreasing region width is proportional to Δ_p. The FORTEC calculation shows qualitatively the same decreasing tendency of χ_i though it is somewhat weaker compared with Lagrangian theory. In conclusion, the reduction of χ_i around the magnetic axis can be explained by the existence of potato particles which is not considered in standard neoclassical theory.

Next example is GAM oscillation and damping. By a similar mechanism of Landau damping, GAM damps if $q \simeq 1$. Though the damping occurs even in the local transport model as in [18] by solving the kinetic equation only on the sole flux surface, the oscillation of E_r on neighboring surfaces are expected to couple through the particle motion passing these surfaces. The simulation results by FORTEC-3D are shown in Fig. 2 and 3 for a reversed-shear configuration $q_{axis} = 3$, $q_{min} = 1.2$ at $r = 0.5$, and $q_{edge} = 8$, varying banana width by changing B and T_i. A strong coupling effect can be seen in large-width case where the damping of E_r oscillation occurred on the resonant surface $r \sim 0.5$ affects the time evolution of E_r on inner and outer surfaces. On the other hand, GAM oscillation on each flux surface seems to be decoupled in the small-width case. The beat patterns of the oscillation amplitude seen in these figures are also explained by the coupling effect of GAM oscillation because the GAM frequency varies in space proportional to thermal velocity on each surfaces. Thus the global evolution of GAM oscillation is found to have a non-local dependency if the orbit scale is large.

4. Transport simulation in 3D configurations

As a benchmark of our hybrid model combining FORTEC-3D and GSRAKE, we show here a simulation results in a LHD-like configuration . The simulation parameters are $R_{axis} = 3.7m$, $\beta_{axis} = 0.08\%$, $B_0 = 1.6T$, and whole plasma region is well in the LMFP (plateau - $1/\nu$) regime. The table of $\Gamma_e(E_\rho, \rho)$ calculated from GSRAKE is shown in Fig. 4. By referring the table, FORTEC-3D solves time evolution of radial electric field and neoclassical transport for ions. In Fig. 5, the contour plot of radial electric field in the (ρ, t) plane is shown. The ι profile is monotonically increasing and it has $\iota = 1$ surface at $\rho \simeq 0.8$. GAM ocsillation is strongly damped there and never appears at $\rho > 0.8$, while the oscillation sustains long time at the inner region. Therefore, the relaxation time scale of E_r and Γ_i to a steady, ambipolar state varies in radial direction depending on the rotational transform profile. The ambipolar electric field at the steady state is shown in Fig. 6. In GSRAKE we can calculate Γ_i as well as Γ_e and ambipolar electric field can be predicted by seeking the roots satisfies $\Gamma_e = \Gamma_i$. It is also shown in Fig. 6. In the present case only one negative root is found in the entire region. These two simulation results show a little different ambipolar E_r. The ion flux calculated in FORTEC-3D contains several effects which is neglected in calculating Γ_i in GSRAKE such as the FOW effects, neoclassical polarization drift in a time-dependent field, energy-scattering in collision term, and orbit loss at the boundary, etc. These differences are considered to be attributed to the difference in Γ_i(FORTEC-3D) and Γ_i(GSRAKE) as large as several tens % seen in the simulation result, and it leads to the difference in the ambipolar electric field profile.

5. Summary

We have developed a global neoclassical transport simulation code FORTEC-3D which is applicable both to axisymmetric and non-axisymmetric toroidal configurations including the finite-orbit-width effect and self-consistent time evolution of radial electric field. By using it, we have demonstrated several transport phenomena which contains non-local effects both in tokamak and stellarator plasmas. It is a promissing tool to investigate non-local transport phenomena and global transport dynamics. We are planning to utilize the simulation system to reveal the non-local process in the evolution of ambipolar electric field in LHD plasmas including the bifurcation phenomenon.

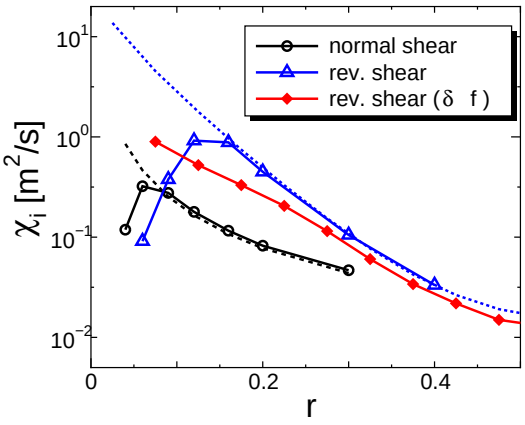

FIG. 1: χ_i calculated in normal and reversed shear configurations from Lagrangian neoclassical theory. Dotted lines are fitting formula by Chang and Hinton. The line with diamonds is a result from FORTEC-3D.

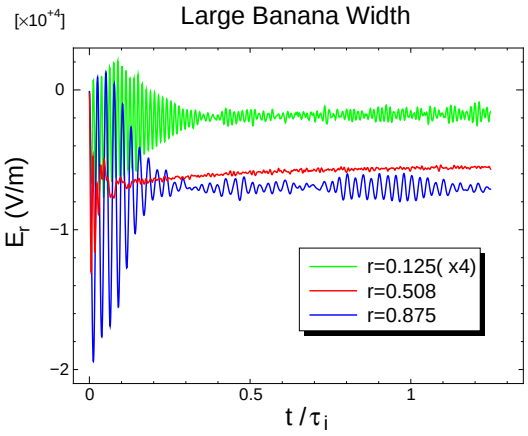

FIG. 2: Time evolution of E_r on three radial positions in a reversed-shear tokamak, $q_{min} = 1.2$ at $r = 0.5$. The typical banana orbit width $\Delta r \sim 10$ cm.

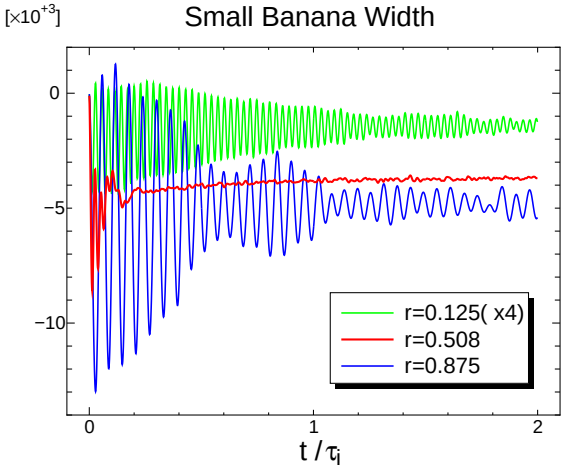

FIG. 3: Time evolution of E_r in the same configuration as in Fig. 1 but Δ_r is about 1/3 times narrower by changing the strength of B-field and ion temperature.

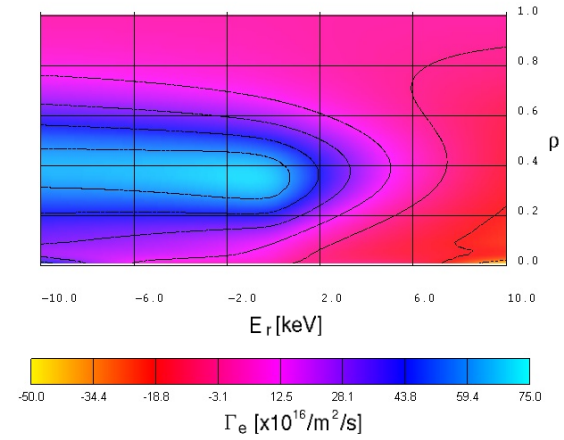

FIG. 4: Electron particle flux in a LHD-like configuration from GSRAKE.

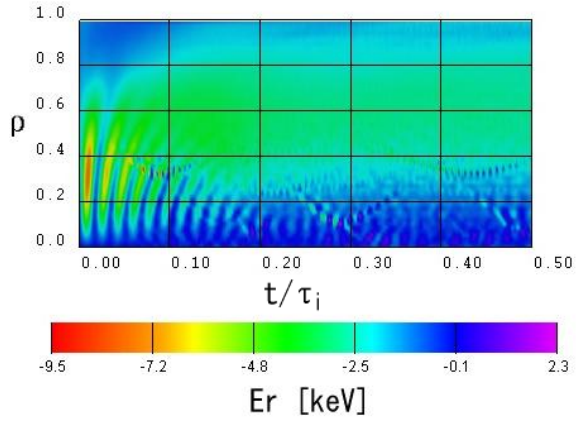

FIG. 5: Time evolution of E_r in a LHD-like configuration calculated by coupling FORTEC-3D and GSRAKE.

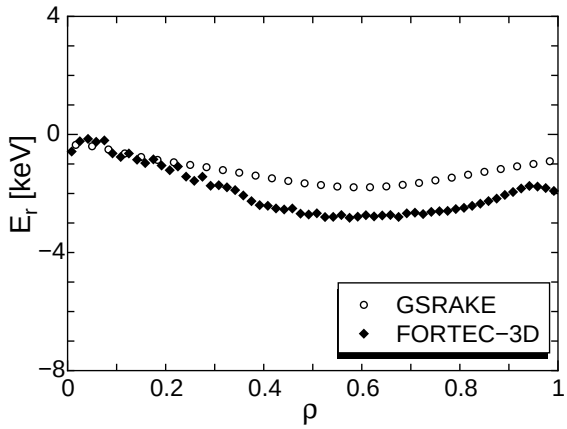

FIG. 6: Comparison of ambipolar electric field profile. Open circles are predicted from GSRAKE and diamonds are the result from FORTEC-3D when it reached a steady state.

References

[1] HINTON, F. L. and HAZELTINE, R. D., Rev. Mod. Phys. **48** (1976) 239.
[2] HIRSHMAN, S. P. and SIGMAR, D. J., Nuclear Fusion **21** (1981) 1079.
[3] SATAKE, S., et al., Journal. Plasma. Fusion Res. **77** (2001) 573.
[4] KOVRIZHNYKH, L. M., Nulc. Fusion **24** (1984) 851.
[5] SHAING, K. C. and CALLEN, J. D., Phys. Fluids **26** (1983) 3315.
[6] WANG, W. X., et al., Plasma Phys. Control. Fusion **41** (1999) 1091.
[7] OKAMOTO, M., et al., Journal of Plasma and Fusion Research **78** (2002) 1344.
[8] HIRSHMAN, S. P. and Betancourt, O., J. Comput. Phys. **96** (1991) 99.
[9] BEIDLER, C. D. and MAAßBERG, H., Plasma Phys. Control. Fusion **43** (2001) 1131.
[10] SATAKE, S., et al., Phys. Plasmas **9** (2002) 3946.
[11] LIN, Z., et al., Phys. Plasmas **2** (1995) 2975.
[12] SUGAMA, H, and NISHIMURA, S, Phys. Plasmas **9** (2002) 4637.
[13] BRUNNER, S., et al., Phys. Plasmas **6** (1999) 4504.
[14] LIN, Z., et al., Phys. Plasmas **4** (1997) 1707.
[15] BERGMANN, A., et al., Phys. Plasmas **8** (2001) 5192.
[16] BERNSTEIN, I. B. and MOLVIG, K., Phys. Fluids **26** (1983) 1488.
[17] CHANG, C. H. and HINTON, F. L., Phys. Fluids **25** (1982) 1493.
[18] NOVAKOVSKII, S. V., et al., Phys. Plasmas **4** (1997) 4272.